# Joint Grid Topology Reconfiguration and Design of Watt-VAR Curves for DERs

Manish K. Singh[1], Sina Taheri[2], Vassilis Kekatos[2], Kevin P. Schneider[3], and Chen-Ching Liu[2]
[1]Dept. of ECE, University of Minnesota, Minneapolis, MN 55455, USA; msingh@umn.edu
[2]Bradley Dept. of ECE, Virginia Tech, Blacksburg, VA 24061, USA; {sinataheri,kekatos,ccliu}@vt.edu
[3]Battelle Seattle Research Center, Pacific Northwest National Laboratory, Seattle, WA 98109, USA; kevin.schneider@pnnl.gov

***Abstract*—Operators can now remotely control switches and update the control settings for voltage regulators and distributed energy resources (DERs), thus unleashing the network reconfiguration opportunities to improve grid efficiency. Aligned to this direction, this work puts forth a comprehensive toolbox of mixed-integer linear programming (MILP) models leveraging the control capabilities of smart grid assets. It develops detailed practical models to capture the operation of locally and remotely controlled regulators, and customize the watt-var DER control curves complying with the IEEE 1547 mandates. Maintaining radiality is a key requirement germane to various feeder optimization tasks. This requirement is accomplished here through an intuitive and provably correct formulation. To our knowledge, this is the first time to optimally select a feeder topology and simultaneously design DER settings while taking into account legacy grid apparatus. The developed toolbox is put into action to reconfigure a grid for minimizing losses using real-world data on a benchmark feeder. The results corroborate that optimal topologies vary across the day and coordinating DERs and regulators is critical during periods of steep net load changes.**

***Index Terms*—Watt-var control; radiality (tree) constraints; voltage regulators; IEEE 1547; linearized distribution flow.**

## I. Introduction

Distribution grids typically operate as radial networks. They are equipped with normally-open switches that allow changes in the network topology and maintain radiality for protection system simplicity. The ability to switch between different topologies brings about a class of grid optimization tasks termed as *distribution network reconfiguration* (DNR), including post-outage restoration, voltage regulation, and power loss minimization [1], [2]. Utilizing existing switches to enhance efficiency and reliability of distribution systems is promising, making DNR a long-pursued task [2], [3]. Network reconfiguration problems are combinatorial in nature, and inevitably introduce integer variables when posed as mathematical programs. However, advancements in mixed-integer solvers revived attempts towards efficient DNR reformulations [4], [5].

The advent of DERs and flexible loads has directed recent DNR research at maximally utilizing the available infrastructure [6], [7]. On the other hand, the intermittency introduced by DERs increases the importance of DNR towards maintaining voltages within safe limits. Thus, attempts are being directed towards leveraging smart grid assets such as dispatchable DERs, capacitor banks, and remotely controlled voltage regulators in DNR formulations. Yet several smart grid devices (such as photovoltaics (PVs) or energy storage units) and legacy grid devices alike operate based on local control rules [8]. On an operational basis, these rules could be fixed (regulators and capacitors) or reconfigured periodically [9]. This is to reduce the frequency in communication and OPF computations. Yet the outcome of DNR could be significantly affected by inaccurate or inadequate modeling of such locally controlled devices. The attempts at proper modeling of these devices are limited and based on simplifying assumptions, such as fixed and known taps for regulators and unity power factor DERs [6]. Enforcing radiality is another critical aspect in grid topology reconfiguration and other optimization tasks, such as planning and topology identification [10]. The popular approaches to enforce radiality include an exhaustive loop elimination, imposing a single inflow edge or a single parent per bus [11], [12], but fail or lack optimality guarantees in the presence of DERs [11].

The contribution of this work is threefold: *i)* Put forth a novel mixed-integer linear program (MILP) model for designing watt-var curves for DERs that takes into account all IEEE 1547 standard mandates; *ii)* Revisit an optimization model for guaranteeing radiality of a feeder to provide a more compact form; and *iii)* Develop an optimization model for capturing the operation of locally controlled regulators. This is in contrast to existing schemes where regulators are either ignored or their taps are presumed known. The proposed DNR is formulated as a mixed-integer quadratic program (MIQP) and tested using real-world data on the IEEE 37-bus grid. Numerical tests corroborate that depending on the load-generation mix experienced across a day, the operator has to select different topologies and regulator/DER settings.

## II. Problem Statement and Existing Models

Suppose a utility knows the feeder model as well as the anticipated load and solar generation on a per-bus basis for the upcoming period of 4 hours or so. The operator would like to reconfigure the grid via remotely controlled switches to minimize ohmic losses. A key requirement is that the reconfigured topology has to remain radial at all times. In addition to switches, the operator can change the tap settings of remotely controlled regulators and select the watt-var curves of DERs to ensure that voltages and line flows remain within specified limits. This section reviews existing models for feeders, nodal/edge constraints, and voltage-dependent loads.

*1) Nodal Variables and Constraints:* A single-phase distribution system with $N+1$ buses can be modeled as a graph $\mathcal{G}(\mathcal{N}_0, \mathcal{E})$. The nodes in $\mathcal{N}_0 := \{0, \ldots, N\}$ correspond to buses; and its directed edges $\mathcal{E}$ to lines, regulators, and switches. The non-substation buses are contained in $\mathcal{N} := \mathcal{N}_0 \setminus \{0\}$. The load-buses are in $\mathcal{N}_\ell \subseteq \mathcal{N}$. Let $v_i$ represent the voltage magnitude and $p_i + jq_i$ the complex power injection at bus $i$. Vectors $\mathbf{v}$ and $\mathbf{p} + j\mathbf{q}$ stack the voltages and injections, respectively, for nodes in $\mathcal{N}$.

A distribution grid may host different types of loads and DERs, such as (in)elastic ZIP loads and (non)dispatchable DERs. The constraints on voltage and power injection for all nodes can be abstractly expressed as

$$\underline{v}\mathbf{1} \leq \mathbf{v} \leq \bar{v}\mathbf{1} \tag{1a}$$

$$\underline{\mathbf{p}}(\mathbf{v}) \leq \mathbf{p} \leq \bar{\mathbf{p}}(\mathbf{v}) \tag{1b}$$

$$\underline{\mathbf{q}}(\mathbf{v}, \mathbf{p}) \leq \mathbf{q} \leq \bar{\mathbf{q}}(\mathbf{v}, \mathbf{q}) \tag{1c}$$

where voltage limits at the point of service are typically set within $\pm 3\%$ per unit (pu) [13]. The functions $\underline{\mathbf{p}}(\mathbf{v})$, $\bar{\mathbf{p}}(\mathbf{v})$, $\underline{\mathbf{q}}(\mathbf{v}, \mathbf{p})$, and $\bar{\mathbf{q}}(\mathbf{v}, \mathbf{q})$ apply entrywise, and depend on load and DER characteristics. Regarding loads, in steady-state analysis the voltage dependence of loads is captured by the ZIP model. Given bus voltage magnitude $v_i$, the power injection of load $i$ is modeled as $p_i(v_i) = \alpha_0^p + \alpha_1^p v_i + \alpha_2^p v_i^2$ and $q_i(v_i) = \alpha_0^q + \alpha_1^q v_i + \alpha_2^q v_i^2$, with all $\alpha$ coefficients being non-positive and assumed known [13]. Linearizing the quadratic dependence of ZIP loads around the nominal voltage of 1 pu, we approximate $v_i^2 \simeq 2v_i - 1$. Then, for all buses hosting loads, the re/active power limits of (1c) can be compactly written as

$$[\underline{p}_i(v_i) \;\; \bar{p}_i(v_i) \;\; \underline{q}_i(v_i) \;\; \bar{q}_i(v_i)]^\top = \boldsymbol{\alpha_0} + v_i \boldsymbol{\alpha_{12}}, \; \forall i \in \mathcal{N}_\ell. \tag{2}$$

If load $i$ is inelastic, then apparently $\underline{p}_i(v_i) = \bar{p}_i(v_i)$; and $\underline{p}_i(v_i) \leq \bar{p}_i(v_i)$ otherwise. Similarly for reactive power injections. Modeling of DERs is deferred to Section III.

*2) Edge Variables and Constraints:* The edge set $\mathcal{E}$ can be partitioned into the set of switches $\mathcal{E}_S$; regulators $\mathcal{E}_R$; and fixed lines $\mathcal{E} \setminus (\mathcal{E}_R \cup \mathcal{E}_S)$. The basic DNR task aims at selecting a subset of switches to be closed. To capture which switches are closed, let us introduce the binary variables $y_e$'s for all switchable lines $e \in \mathcal{E}_S$. Variable $y_e = 1$ indicates that switch $e$ is closed or connected; and vice versa. The power flow $P_e + jQ_e$ on edge $e$ is constrained as

$$y_e[\underline{P}_e \;\; \underline{Q}_e] \leq [P_e \;\; Q_e] \leq y_e[\bar{P}_e \;\; \bar{Q}_e], \; \forall \; e \in \mathcal{E} \tag{3a}$$

where $y_e$ is a variable for switches; and is fixed to 1 for lines and regulators. If switch $e$ is open ($y_e = 0$), constraint (3a) sets the power flow on $e$ to zero. Else, box constraints on the power flow are enforced and usually $\underline{P}_e = -\bar{P}_e$ and $\underline{Q}_e = -\bar{Q}_e$.

*3) Linearized Distribution Flow (LDF) Model:* Per the LDF model, the power injections at each bus $i$ are [2]:

$$p_i = \sum_{e:(i,j)\in\mathcal{E}} P_e - \sum_{e:(j,i)\in\mathcal{E}} P_e \tag{4a}$$

$$q_i = \sum_{e:(i,j)\in\mathcal{E}} Q_e - \sum_{e:(j,i)\in\mathcal{E}} Q_e. \tag{4b}$$

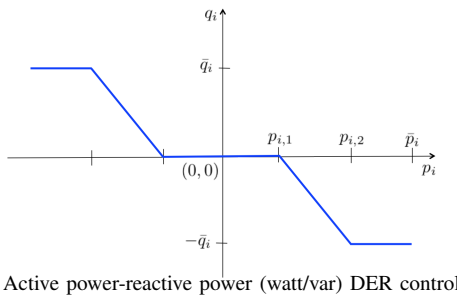


Fig. 1. Active power-reactive power (watt/var) DER control curve.

If $r_e + jx_e$ is the impedance of line $e : (i,j) \in \mathcal{E}$, the LDF model relates the *squared* voltage magnitudes to power flows linearly as $v_i^2 - v_j^2 = 2r_eP_e + 2x_eQ_e$. Using the linearization $v_i^2 \simeq 2v_i - 1$ in the LDF model, one obtains [14]

$$v_i - v_j = r_eP_e + x_eQ_e, \quad \forall \; e : (i,j) \in \mathcal{E} \setminus (\mathcal{E}_R \cup \mathcal{E}_S). \tag{5}$$

For switchable lines in $\mathcal{E}_S$, the voltage drop of (5) applies only if the switch is closed, that is

$$y_e(v_i - v_j - r_eP_e - x_eQ_e) = 0, \quad \forall \; e : (i,j) \in \mathcal{E}_S. \tag{6}$$

The bilinear products appearing in (6) such as $y_ev_i$ are handled using McCormick linearization [15]; see also [16].

## III. Designing Watt-Var Control Curves for DERs

The IEEE 1547 standard mandates DERs to provide reactive power support according to four possible modes: *i)* constant power factor; *ii)* voltage-dependent reactive power (volt-var); *iii)* active power-dependent reactive power (watt-var); and *iv)* constant reactive power mode. The watt-var dependencies are captured by control rules described by piecewise affine functions; see Fig. 1. To effectively integrate DERs, these rules should be decided optimally based on feeder and loading conditions. We henceforth assume that DERs are operating in the watt-var mode and their parameters are adjusted routinely.

To simplify the exposition, we consider DERs operating in the right halfspace of the watt-var rule of Fig. 1 (e.g., generation). Given the rated reactive power capacity $\bar{q}_i$ for the $i$-th DER, the controllable parameters are $p_{i,1}$ and $p_{i,2}$. The IEEE 1547 standard further constraints $(p_{i,1}, p_{i,2})$ as

$$0.4\bar{p}_i \leq p_{i,1} \leq 0.8\bar{p}_i \tag{7a}$$

$$p_{i,1} + 0.1\bar{p}_i \leq p_{i,2} \leq \bar{p}_i \tag{7b}$$

where $\bar{p}_i$ is the rated active power for DER $i$. These specifications are set by the standard to ensure a substantial deadband and to avoid steep slopes in Fig. 1. Given $(p_{i,1}, p_{i,2})$, the reactive power of DER $i$ depends on its active power as

$$q_i(p_i) = \begin{cases} 0 & , \; 0 \leq p_i \leq p_{i,1} \\ \frac{-\bar{q}_i(p_i - p_{i,1})}{p_{i,2} - p_{i,1}} & , \; p_{i,1} \leq p_i \leq p_{i,2} \\ -\bar{q}_i & , \; p_{i,2} \leq p_i \leq \bar{p}_i \end{cases} \tag{8}$$

The control rule of (8) induces a non-linear equality constraint between variables $q_i$, $p_{i,1}$, and $p_{i,2}$, which we next capture by a novel MILP model: Introduce three binary variables to indicate which of the three segments in (8) is active each time

$$(\delta_{i,1}, \delta_{i,2}, \delta_{i,3}) \in \{0,1\}^3 \;\; \text{and} \;\; \delta_{i,1} + \delta_{i,2} + \delta_{i,3} = 1. \tag{9}$$

The selection of a segment depends on the value of $p_i$ as

$$\delta_{i,2}p_{i,1} + \delta_{i,3}p_{i,2} \leq p_i \leq \delta_{i,1}p_{i,1} + \delta_{i,2}p_{i,2} + \delta_{i,3}\bar{p}_i. \quad (10)$$

Then, the rule of (8) can be expressed by the constraint

$$q_i = \delta_{i,1} \cdot 0 - \delta_{i,2}\frac{\bar{q}_i(p_i - p_{i,1})}{p_{i,2} - p_{i,1}} - \delta_{i,3}\bar{q}_i. \quad (11)$$

Albeit (10) involves binary-continuous variable products, and can be thus handled by MacCormick linearization, that is not the case for (11). Unfortunately, the latter entails ratios or products of continuous variables. To bypass this difficulty, we parameterize Fig. 1 using the slope/intercept of its middle segment instead of the breakpoints $(p_{i,1}, p_{i,2})$. If the middle segment of (8) is denoted by $q_i(p_i) = \beta_i p_i + \gamma_i$ for some negative $(\beta_i, \gamma_i)$, then (11) is equivalent to

$$q_i = \delta_{i,2}(\beta_i p_i + \gamma_i) - \delta_{i,3}\bar{q}_i. \quad (12)$$

Different from (10), constraint (12) involves only binary-continuous variable products. We next reformulate (10) in terms of $(\beta_i, \gamma_i)$. Because the line $q_i(p_i) = \beta_i p_i + \gamma_i$ passes through the points $(p_{i,1}, 0)$ and $(p_{i,2}, -\bar{q}_i)$, we get that

$$p_{i,1} = -\frac{\gamma_i}{\beta_i} \quad \text{and} \quad p_{i,2} = -\frac{\bar{q}_i + \gamma_i}{\beta_i}. \quad (13)$$

Plugging (13) into (10); multiplying all sides by $\beta_i < 0$; adding $\gamma_i$; and using (9), eventually provides

$$\delta_{i,3}(\gamma_i - \beta_i\bar{p}_i) - \delta_{i,2}\bar{q}_i \leq \beta_i p_i + \gamma_i \leq \delta_{i,1}\gamma_i - \delta_{i,3}\bar{q}_i \quad (14)$$

which is still amenable to McCormick linearization.

The rule of (8) is equivalent to (9), (12), and (14). With the help of McCormick linearization, the latter can be posed as an MILP model. The aforesaid model captures the piecewise rule, but does not enforce the limitations of (7). To capture those, we translate the constraints on $(p_{i,1}, p_{i,2})$ to constraints on $(\beta_i, \gamma_i)$. Plugging (13) into (7) implies $(\beta_i, \gamma_i)$ should satisfy

$$-0.4\bar{p}_i\beta_i \leq \gamma_i \leq -0.8\bar{p}_i\beta_i \quad (15a)$$

$$\bar{p}_i\beta_i + \gamma_i \leq -\bar{q}_i \leq 0.1\bar{p}_i\beta_i. \quad (15b)$$

To summarize, the control rule for DER $i$ is optimally tuned via variables $(\beta_i, \gamma_i)$ that satisfy (9), (12), (14), and (15). To the best of our knowledge, this is the first model to optimally design the IEEE 1547 control curves for DERs.

## IV. Modeling Voltage Regulators

A regulator scales its secondary-side voltage by $\pm 10\%$ in increments of $0.625\%$ using tap positions [8]. Consider a regulator modeled by edge $e : (i, j) \in \mathcal{E}_R$. Its voltage transformation ratio can be set to $1 + 0.00625 \cdot t_e$, where $t_e \in \{0, \pm 1, \ldots, \pm 16\}$ is its tap position. We consider locally and remotely controlled regulators [13]. A locally controlled regulator aims to maintain $v_j$ within a given range $[\underline{v}_j, \bar{v}_j]$. The regulator changes its taps after a time delay until $v_j$ is brought within $[\underline{v}_j, \bar{v}_j]$, unless an extreme tap position has been reached. Ignoring the time delay, this operation is shown in Figure 2 and described by

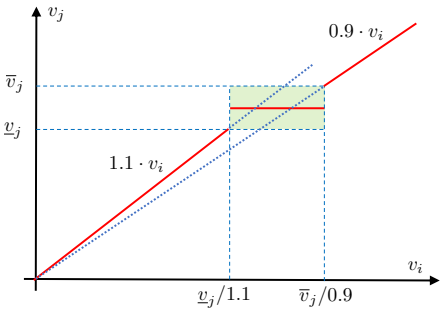


Fig. 2. Locally controlled regulator characteristic: The left/rightmost segments occur when regulator taps have maxed out. Within the middle green box, the secondary voltage is successfully regulated. Lacking the actual tap position, this middle area is approximated by its midpoint (reference voltage).

$$v_j(v_i) = \begin{cases} 1.1 \cdot v_i & , \ v_i \leq \frac{\underline{v}_j}{1.1} \\ [\underline{v}_j, \bar{v}_j] & , \ \frac{\underline{v}_j}{1.1} < v_i < \frac{\bar{v}_j}{0.9} \\ 0.9 \cdot v_i & , \ v_i \geq \frac{\bar{v}_j}{0.9} \end{cases}. \quad (16)$$

The first branch relates to the case where the primary voltage $v_i$ is quite low and even with $t_e = +16$, the secondary voltage $v_j = 1.1 \cdot v_i$ remains below $\underline{v}_j$. Likewise, the third branch relates to the case where the tap has reached its minimum of $t_e = -16$. Normal operation is captured by the second branch, where $v_j$ is successfully regulated within $[\underline{v}_j, \bar{v}_j]$.

As the operator cannot fully monitor and/or control the exact tap position, we propose approximating the second branch of (16) by setting $v_j$ at the mid-point of the range

$$v_j(v_i) = \frac{\bar{v}_j + \underline{v}_j}{2} \quad \text{when} \quad v_i \in \left(\frac{\underline{v}_j}{1.1}, \frac{\bar{v}_j}{0.9}\right).$$

Since the regulation range typically spans 2–4 taps or 0.0125–0.025 pu [8], this approximation incurs negligible modeling error. The approximate operation of Fig. 2 can be modeled similarly to the watt-var curve of (8), using three binary variables selecting the three regions of operation:

$$v_i \geq 0.8\delta_{e,1} + \frac{\underline{v}_j}{1.1}\delta_{e,2} + \frac{\bar{v}_j}{0.9}\delta_{e,3} \quad (17a)$$

$$v_i \leq \frac{\underline{v}_j}{1.1}\delta_{e,1} + \frac{\bar{v}_j}{0.9}\delta_{e,2} + 1.2\delta_{e,3} \quad (17b)$$

$$v_j = 1.1\delta_{e,1}v_i + \delta_{e,2}\left(\frac{\bar{v}_j + \underline{v}_j}{2}\right) + 0.9\delta_{e,3}v_i \quad (17c)$$

$$\delta_{e,1} + \delta_{e,2} + \delta_{e,3} = 1, \ \text{and} \ (\delta_{i,1}, \delta_{i,2}, \delta_{i,3}) \in \{0, 1\}^3 \quad (17d)$$

The binary-continuous variable products in (17c) can be handled via McCormick linearization. For remotely controlled regulators, their taps can be changed remotely and hence, their voltage ratio becomes an optimization variable taking one of 33 possible values. This can be encoded using the 6-bit binary expansion model of [17].

## V. Ensuring Radial Topologies

Ensuring a graph is radial is of central importance to various grid tasks. In grids with a single power source and no DERs, enforcing radiality entails allowing one incoming flow edge

per bus [4]. With DERs present, a bus may receive power from multiple edges even for radial grid. To handle such networks, the model of [5] enforces an edge orientation so that each bus has a single parent bus. However, counterexamples where this parent-child model produces disconnected graphs do exist [12]. A dual graph-based model was suggested in [12], but is limited to planar graphs. For a general network, cycles can be avoided by constraining the number of connected edges on each cycle to be less than the cycle length [7]. Despite its generality, this cycle-elimination approach can lead to exponentially many constraints. One of the most popular radiality model ensures connectivity of loads to DERs via the power flow equations, and connects DERs to the substation via flows of a virtual commodity [11]. We build upon the commodity flow approach and propose a more succinct model with fewer variables and constraints.

Given the complete graph $\mathcal{G}(\mathcal{N}_0, \mathcal{E})$, define a subgraph $\check{\mathcal{G}}(\mathcal{N}_0, \check{\mathcal{E}})$, such that $\check{\mathcal{E}} := \mathcal{E} \setminus \{e : e \in \mathcal{E}_S, y_e = 0\}$. The subgraph $\check{\mathcal{G}}$ represents the reconfigured network. To capture the line infrastructure of $\mathcal{G}$, define its $|\mathcal{E}| \times (N+1)$ branch-bus incidence matrix $\tilde{\mathbf{A}}$. Its $(e,i)$-th entry takes the value of $+1$ $(-1)$ if edge $e \in \mathcal{E}$ starts (ends) at bus $i$; and 0, otherwise. Separate the first column $\mathbf{a}_0$ of $\tilde{\mathbf{A}}$ related to the substation as $\tilde{\mathbf{A}} = [\mathbf{a}_0 \ \mathbf{A}]$, to get the *reduced* incidence matrix $\mathbf{A}$. Similarly, let $\check{\mathbf{A}} \in \mathbb{R}^{|\check{\mathcal{E}}| \times N}$ represent the reduced branch-bus incidence matrix of subgraph $\check{\mathcal{G}}$. The next claim (shown in [16]) establishes a model for imposing graph connectivity.

**Proposition 1.** *([16]) A graph $\check{\mathcal{G}}(\mathcal{N}_0, \check{\mathcal{E}})$ with reduced branch-bus incidence matrix $\check{\mathbf{A}}$ is connected if and only if there exists a vector of virtual flows $\mathbf{f} \in \mathbb{R}^{|\check{\mathcal{E}}|}$, such that $\check{\mathbf{A}}^\top \mathbf{f} = \mathbf{1}$.*

Proposition 1 involves $\check{\mathbf{A}}$, which depends on the switch statuses $y_e$'s. Notice that $\check{\mathbf{A}}$ is derived from $\mathbf{A}$ by removing the rows related to open switches. Therefore, the condition of Prop. 1 can be expressed with respect to the original $\mathbf{A}$, by forcing the virtual flows in $\mathbf{f}$ to be zero for open lines.

**Corollary 1.** *Let $\mathbf{A}$ be the reduced branch-bus incidence matrix of $\mathcal{G}$, and $\check{\mathcal{G}} \subseteq \mathcal{G}$ be a subgraph defined by opening switches $\{e \in \mathcal{E}_S : y_e = 0\}$. Subgraph $\check{\mathcal{G}}$ is connected if and only if there exists $\mathbf{f} \in \mathbb{R}^{|\mathcal{E}|}$ such that*

$$\mathbf{A}^\top \mathbf{f} = \mathbf{1} \quad \text{and} \quad -y_e N \leq f_e \leq y_e N, \quad \forall e \in \mathcal{E}_S. \tag{18}$$

Constraint (18) implies that the virtual flows on open switches are zero, and bounds the flows on closed switches within $[-N, \ N]$. Once a graph $\check{\mathcal{G}}$ is ensured to be connected, the requirement of radiality can be readily enforced as

$$\sum_{e \in \mathcal{E}_S} y_e = N - |\mathcal{E} \setminus \mathcal{E}_S| \tag{19}$$

to ensure the total number of connected edges is $N$.

## VI. Problem Formulation

W can now formulate the optimal DNR task. Consider an operating period of 4 hr. Before the start of this period, the operator collects minute-based data capturing the anticipated load and solar generation, and partition them into 15-min intervals. From each 15-min interval, the operator selects $S$ samples, yielding a total of $T = 16S$ samples for the upcoming 4-hr period, indexed by $t$. The data related to sample $t$ are collectively denoted by vector $\boldsymbol{\theta}^t$. The operator would like to minimize the total power losses summed over $T$ instances. Although each one of the $T$ instances experiences different loading conditions, they all share the same feeder topology and DER/regulator settings. To capture this, we group optimization variables as

$$\boldsymbol{\omega}_1 := \{\{y_e\}_{e \in \mathcal{E}_S}, \{\beta_i, \gamma_i\}_{i \in \mathcal{N} \setminus \mathcal{N}_\ell}, \{b_{e,k}\}_{e \in \mathcal{E}_R \setminus \mathcal{E}_R^L}\}; \text{ and}$$
$$\boldsymbol{\omega}_2^t := \{\mathbf{v}^t, \mathbf{p}^t, \{q_i^t, \delta_{i,k}^t\}_{i \in \mathcal{N} \setminus \mathcal{N}_\ell}, \{\delta_{e,k}^t\}_{e \in \mathcal{E}_R^L}, \mathbf{P}^t, \mathbf{Q}^t\}, \ \forall t.$$

The ultimate goal is to determine $\boldsymbol{\omega}_1$. The grid would then be allowed to operate autonomously using local rules per interval $t$ yielding variables $\{\boldsymbol{\omega}_2^t\}_{t=1}^T$. The DNR task can be posed as

$$\min_{\boldsymbol{\omega}_1, \{\boldsymbol{\omega}_2^t\}_{t=1}^T} \ \sum_{t \in \mathcal{T}} \sum_{e \in \mathcal{E} \setminus \mathcal{E}_R} r_e (P_{e,t}^2 + Q_{e,t}^2) \tag{DNR}$$
$$\text{s.to} \quad (1)-(6), (9), (12), (14), (15), (19), (17) \quad \forall t.$$

The objective approximates the ohmic losses along all lines and times per the LDF model.

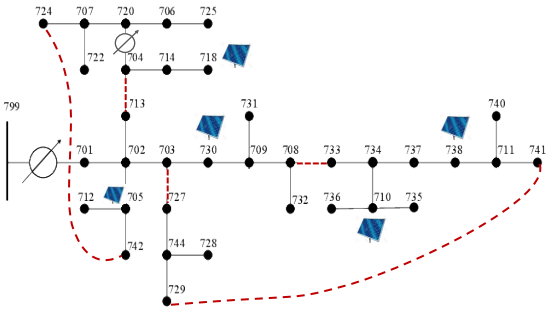


Fig. 3. The IEEE 37-bus feeder with an additional regulator, lines, and DERs.

## VII. Numerical Tests and Conclusions

The developed DNR was tested on a modified IEEE 37-bus feeder converted to its single-phase equivalent; see Fig. 3. Switches include three existing and two additional lines, all denoted as dashed edges. Regulator $(799, 701)$ is assumed to be remotely controlled. The regulator added on line $(704, 720)$ is set locally controlled with reference voltage 1 pu and bandwidth 0.016 pu. Five PVs of equal capacity were placed. Fig. 4 (*left*) shows normalized minute-based load and solar data that were extracted from the Pecan Street dataset [18]; see [16] for details. We synthesized reactive loads by scaling the actual demand to match the nominal benchmark power factors. The linearized ZIP parameters of (2) were found using the derived (re)active load profiles for each bus and the load type from the benchmark. Representing high solar integration, solar data were scaled to meet 75% of the energy consumption. Problem (DNR) was solved using YALMIP and Gurobi [19].

The 24-hr interval was partitioned into five periods $\mathcal{T}_1 - \mathcal{T}_5$; see Fig. 4. Each period was divided into 15-min intervals

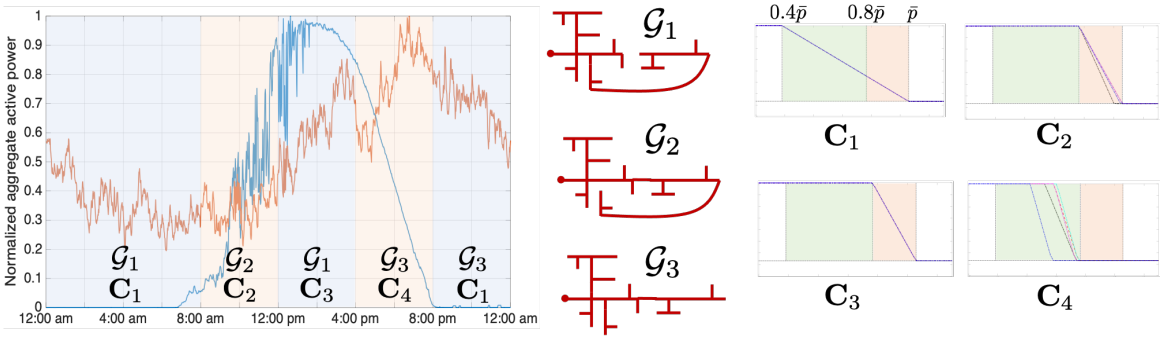


Fig. 4. *left*: Normalized aggregate active load and solar generation over time. The 5 panes represent the operating periods $\mathcal{T}_1 - \mathcal{T}_5$ and $(\mathcal{G}, \mathbf{C})$ labels indicate optimal topology and watt-var curves; *right*: dictionary of obtained optimal topology and watt-var curves.

and $S = 2$ load and generation samples were randomly drawn from the minute-based data. We then solved five instances of (DNR). The optimal topologies and watt-var curves obtained for different periods are shown in Fig. 4. The average power loss incurred during the five periods were $\{1.5, 1.9, 9.9, 4.6, 5.1\} \times 10^{-2}$ and the optimal tap settings were $\{19, 16, 15, 21, 21\}$, respectively. Since period $\mathcal{T}_1$ experiences negligible solar generation, its watt-var curves are inconsequential. During period $\mathcal{T}_2$, while all PVs tend to absorb minimal reactive power and hence hit the limits of the watt-var curve in (7), the PV at bus 738 obtains a different curve and absorbs its maximum reactive power before reaching its $\bar{p}$. During $\mathcal{T}_3$, voltages remain within limits because both load and generation are high, and so watt-var curves coincide with minimal reactive absorption. Period $\mathcal{T}_4$ witnesses a steep variation in load-generation mix. Such variation is tackled via a high tap setting of 21 and relatively aggressive participation in reactive absorption; see curve $\mathbf{C}_4$. Finally, period $\mathcal{T}_5$ with no PV generation yields generic watt-var curves similar to $\mathcal{T}_1$, but different taps and topology due to high load.

We also experimented with the numbers of operating periods and samples $S$. The effects are on three fronts: *i)* Frequency of changes in taps, topology, and inverter curves; *ii)* Voltage violations over *all* minute-based data after fixing $\boldsymbol{\omega}_1$; and *iii)* Total active power loss for *all* minute-based data after fixing $\boldsymbol{\omega}_1$. Shorter periods result in more frequent operations on taps, switches, and inverter settings, while longer periods may render problem (DNR) infeasible due to extreme changes in the load-generation mix. Even when feasible, longer periods lead to increased losses. For a fixed length, increasing $S$ results in lower losses and voltage violations and higher computational burden.

Our numerical tests have corroborated: *a)* The optimal topology varies with the load-generation mix; *b)* Coordinating DERs and regulators is critical during periods of steep transitions; and *c)* The trade-offs involved in the length of operating periods and the number of scenarios. Extending this work to multiphase grids, exact AC grid models, and/or considering volt-var rather than watt-var (which introduce stability concerns) are relevant research directions.

## REFERENCES


[1] C. Chen, J. Wang, and D. Ton, "Modernizing distribution system restoration to achieve grid resiliency against extreme weather events: An integrated solution," *Proc. IEEE*, vol. 105, no. 7, pp. 1267–1288, Jul. 2017.

[2] M. Baran and F. Wu, "Network reconfiguration in distribution systems for loss reduction and load balancing," *IEEE Trans. Power Delivery*, vol. 4, no. 2, pp. 1401–1407, Apr. 1989.

[3] C. C. Liu, S. J. Lee, and S. S. Venkata, "An expert system operational aid for restoration and loss reduction of distribution systems," *IEEE Trans. Power Syst.*, vol. 3, no. 2, pp. 619–626, May 1988.

[4] J. A. Taylor and F. S. Hover, "Convex models of distribution system reconfiguration," *IEEE Trans. Power Syst.*, vol. 27, no. 3, pp. 1407–1413, Aug. 2012.

[5] R. A. Jabr, R. Singh, and B. C. Pal, "Minimum loss network reconfiguration using mixed-integer convex programming," *IEEE Trans. Power Syst.*, vol. 27, no. 2, pp. 1106–1115, May 2012.

[6] B. Chen, C. Chen, J. Wang, and K. L. Butler-Purry, "Sequential service restoration for unbalanced distribution systems and microgrids," *IEEE Trans. Power Syst.*, vol. 33, no. 2, pp. 1507–1520, Mar. 2018.

[7] M. K. Singh, V. Kekatos, and C.-C. Liu, "Optimal distribution system restoration with microgrids and distributed generators," in *Proc. IEEE PES General Meeting*, Atlanta, GA, Aug. 2019.

[8] J. A. Kersulis and I. A. Hiskens, "Renewable voltage regulation and the transformer tapping trade-off," in *Proc. IEEE Conf. on Innovative Smart Grid Technologies*, Melbourne, Australia, Nov. 2016.

[9] M. Jalali, V. Kekatos, N. Gatsis, and D. Deka, "Designing reactive power control rules for smart inverters using support vector machines," *IEEE Trans. Smart Grid*, vol. 11, no. 2, pp. 1759 – 1770, Mar. 2020.

[10] S. Taheri, V. Kekatos, and G. Cavraro, "An MILP approach for distribution grid topology identification using inverter probing," in *Proc. IEEE PowerTech*, Milan, Italy, Jun. 2019, pp. 1–6.

[11] S. Lei, C. Chen, Y. Song, and Y. Hou, "Radiality constraints for resilient reconfiguration of distribution systems: Formulation and application to microgrid formation," *IEEE Trans. Smart Grid*, vol. 11, no. 5, pp. 3944 – 3956, Sep. 2020.

[12] H. Ahmadi and J. R. Marti, "Mathematical representation of radiality constraint in distribution system reconfiguration problem," *International J. Electrical Power & Energy Systems*, vol. 64, pp. 293 – 299, 2015.

[13] W. H. Kersting, *Distribution System Modeling and Analysis*. New York, NY: CRC Press, 2001.

[14] S. Taheri, M. Jalali, V. Kekatos, and L. Tong, "Fast probabilistic hosting capacity analysis for active distribution systems," *IEEE Trans. Smart Grid*, vol. 12, no. 3, pp. 2000 – 2012, May 2021.

[15] G. P. McCormick, "Computability of global solutions to factorable nonconvex programs: Part I – Convex underestimating problems," *Mathematical Programming*, vol. 10, no. 1, pp. 147–175, Dec. 1976.

[16] M. K. Singh, S. Taheri, V. Kekatos, K. P. Schneider, and C.-C. Liu, "Joint grid topology reconfiguration and design of watt-var curves for der," Tech. Rep., Feb. 2020. [Online]. Available: https://arxiv.org/abs/1910.03020

[17] W. Wu, Z. Tian, and B. Zhang, "An exact linearization method for OLTC transformers in branch flow model," *IEEE Trans. Power Syst.*, vol. 32, no. 3, pp. 2475–2476, May 2017.

[18] (2013) Pecan Street Inc. Dataport. [Online]. Available: https://dataport.pecanstreet.org/

[19] J. Lofberg, "YALMIP : A toolbox for modeling and optimization in MATLAB," in *Proc. of the CACSD Conf.*, Taipei, Taiwan, 2004.